

# Effect of molecular weight and chain end groups on crystal forms of poly(vinylidene fluoride) oligomers

Herman, Toshiyuki Uno, Astushi Kubono, Susumu Umemoto,  
Takeshi Kikutani and Norimasa Okui\*

*Tokyo Institute of Technology, Department of Organic and Polymeric Materials, Ookayama,  
Meguroku, Tokyo 152, Japan*

*(Received 30 April 1996; revised 6 June 1996)*

The micro-structure of poly(vinylidene fluoride) oligomers was characterized by  $^{19}\text{F}$  and  $^{13}\text{C}$  n.m.r. and the effects of molecular weight and the chain end groups on the crystal forms were studied by i.r. and X-ray methods. One of the oligomers terminated with  $-\text{CH}_3$  and the fragment of an initiator at the chain ends. The other oligomers were terminated with  $-\text{Cl}$  and  $\text{CCl}_3-$  at their chain ends. The larger chain end groups tended to produce the conformational disorder in the molecules yielding the  $\gamma$  form. The smaller molecular weight of the oligomer gave rise to the  $\beta$  form. © 1997 Elsevier Science Ltd. All rights reserved.

**(Keywords: poly(vinylidene fluoride); oligomer; chain end)**

## INTRODUCTION

The crystal form of poly(vinylidene fluoride) (PVDF) can be divided into roughly three forms:  $\alpha$ ,  $\beta$  and  $\gamma$ . The  $\beta$  and the  $\gamma$  forms of PVDF exhibit piezoelectricity, but not the  $\alpha$  form<sup>1</sup>. In general, the  $\alpha$  form can be obtained by crystallizing PVDF from the melt or by casting from acetone solution. The  $\beta$  form can be obtained by drawing and poling PVDF film or by quenching the film from the molten state<sup>2</sup>. The  $\gamma$  form can be prepared by annealing the film at a relatively high temperature.

PVDF is thermally decomposed in a vacuum system when the polymer is heated above 300°C. Low molecular weight fractions (oligomers) in PVDF can be evaporated without thermal decomposition at temperatures below 300°C<sup>3,4</sup>. The molecular weight of VDF oligomers obtained by vapour deposition depends on the deposition conditions, such as evaporation crucible temperature, pressure, distance from the source crucible to the substrate, etc. The molecular orientation and the crystal structure in the films could be controlled by the substrate temperature and the deposition rate<sup>5</sup>. For example, VDF oligomer deposited at substrate temperatures below  $-100^\circ\text{C}$  yields the  $\beta$  form with the molecular orientation parallel to the substrate. The  $\alpha$  form is obtained at a substrate temperature of 25°C with the normal molecular orientation to the substrate.

In this study, we present the characterization of the oligomers obtained from the vapour deposition method and those prepared by telomerization of VDF monomer in the presence of  $\text{CCl}_4$ . The effects of molecular weight and the chain end groups on the crystal form,  $\alpha$ ,  $\beta$  and  $\gamma$ , are studied by i.r. and X-ray methods.

## EXPERIMENTAL

### Samples

Poly(vinylidene fluoride) (PVDF) and three VDF oligomers (A, B and C) were used in this study. PVDF was a commercial sample purchased from Showa Denko Co. Ltd with molecular weight of 88 000. One of the VDF oligomers (sample A) was accumulated from PVDF by the vapour-deposition method at below 300°C where the low molecular weight fractions in PVDF were evaporated without thermal decomposition<sup>3,4</sup>. The other VDF oligomers of B and C samples were kindly supplied from Kureha Co. Ltd. where VDF monomers were telomerized by suspension polymerization method in acetone solution in the presence of  $\text{CCl}_4$  with di-*n*-propyl-peroxy-dicarbonate as a catalyst.

### Measurements

Solution-state  $^{19}\text{F}$  and  $^{13}\text{C}$  n.m.r. were recorded on a JEOL JMN-GX 500 spectrometer operating at 245.05 and 125.65 MHz, respectively.  $^{13}\text{C}$  n.m.r. was measured in broad-band proton decoupling mode. Samples were dissolved in acetone- $d_6$  (99% purity). X-ray diffraction patterns were recorded with a conventional  $\theta - 2\theta$  diffractometer (Rigaku Rad-B). I.r. spectra of the samples were recorded by JASCO Micro F.T.i.r. 100T. Melting and crystallization temperatures for the samples were recorded on a Shimadzu T40 at a heating rate and a cooling rate of  $10^\circ\text{C min}^{-1}$ .

## RESULTS AND DISCUSSION

Figure 1 shows  $^{19}\text{F}$  n.m.r. spectra for PVDF and two oligomers of A and B. According to the reference data

\* To whom correspondence should be addressed

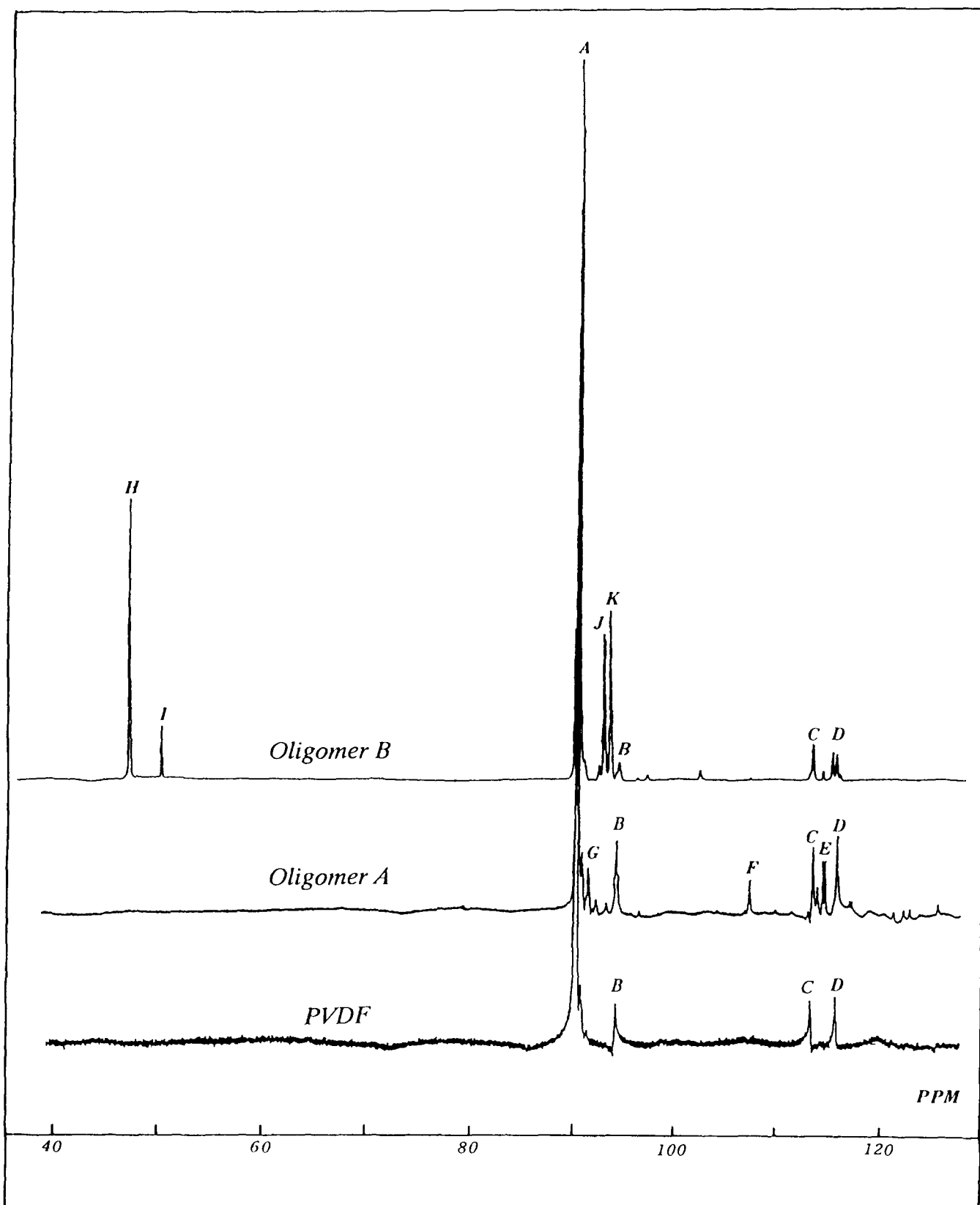


Figure 1  $^{19}\text{F}$  n.m.r. spectra of PVDF and two oligomers A and B

reported elsewhere<sup>6-9</sup>, various peaks denoted by the capital letters from A to K in Figure 1 can be easily assigned. Peak A is associated with the normal head-to-tail (h-t) structure. The peaks of B, C and D correspond to the  $-\text{CF}_2-$  resonances in the head-to-head (h-h) or tail-to-tail (t-t) structures as listed in Table 1. Signals related to the end groups can be easily

identified from the difference in the spectra between PVDF and two oligomers. The peaks of H, I and J in oligomer B are associated with the chemical structures  $-\text{CH}_2\text{CF}_2\text{CH}_2\text{CF}_2-\text{Cl}$ ,  $-\text{CF}_2\text{CH}_2\text{CH}_2\text{CF}_2-\text{Cl}$  and  $-\text{CH}_2\text{CF}_2\text{CH}_2\text{CF}_2\text{Cl}$ , respectively. The peak intensity of I is about 1/6 order of the peak H, indicating the heterogeneous linkages near to the chain ends to

**Table 1** Assignments of  $^{19}\text{F}$  and  $^{13}\text{C}$  n.m.r. resonances of VDF oligomers

Signal in figures	$^{19}\text{F}$ n.m.r.	$^{13}\text{C}$ n.m.r.	
	$-\text{CF}_2-$ $\delta$ (ppm) vs $\text{CFCl}_3$	$-\text{CF}_2-$ $\delta$ (ppm) vs TMS	$-\text{CH}_2-$ $\delta$ (ppm) vs TMS
A, A'	$\rightarrow \text{CH}_2\text{CF}_2 \rightarrow \rightarrow$ -90.7	$\rightarrow \text{CH}_2\text{CF}_2 \rightarrow$ 120.6	$\rightarrow \text{CH}_2\text{CF}_2 \rightarrow$ 44.3
B	$\leftarrow \text{CH}_2\text{CF}_2 \rightarrow \rightarrow$ -94.5		
C	$\rightarrow \text{CH}_2\text{CF}_2 \leftarrow \leftarrow$ -113.2		$\rightarrow \text{CH}_2\text{CF}_2 \leftarrow$ 37.4
D	$\leftarrow \text{CH}_2\text{CF}_2 \leftarrow \leftarrow$ -115.5		$\leftarrow \text{CH}_2\text{CF}_2 \leftarrow$ 23.6
E	$\rightarrow \rightarrow \text{CH}_2\text{CF}_2\text{H}$ -114.1		
F	$\text{CH}_3\text{CF}_2 \rightarrow \rightarrow$ -107.1		
G	$\rightarrow \text{CH}_2\text{CF}_2 \rightarrow \text{H}$ -91.9		
H, H'	$\rightarrow \rightarrow \text{CH}_2\text{CF}_2\text{Cl}$ -47.6	$\rightarrow \rightarrow \text{CH}_2\text{CF}_2\text{Cl}$ 126.7	$\rightarrow \rightarrow \text{CH}_2\text{CF}_2\text{Cl}$ 48.1
I	$\rightarrow \leftarrow \text{CH}_2\text{CF}_2\text{Cl}$ -50.7	$\rightarrow \leftarrow \text{CH}_2\text{CF}_2\text{Cl}$ 130.0	
J	$\rightarrow \text{CH}_2\text{CF}_2 \rightarrow \text{Cl}$ -93.0	$\rightarrow \text{CH}_2\text{CF}_2 \rightarrow \text{Cl}$ 119.5	
K, K'	$\text{CCl}_3\text{CH}_2\text{CF}_2 \rightarrow \rightarrow$ -93.7	$\text{CCl}_3\text{CH}_2\text{CF}_2 \rightarrow \rightarrow$ 120.0	$\text{CCl}_3\text{CH}_2\text{CF}_2 \rightarrow \rightarrow$ 58.8
L			$\text{CCl}_3 \rightarrow \rightarrow$ 93.1

$\rightarrow$ :  $-\text{CH}_2\text{CF}_2-$      $\leftarrow$ :  $-\text{CF}_2\text{CH}_2-$

be about 7%. The peak K can be related to  $-\text{CF}_2-$  terminated with  $\text{CCl}_3-$  end group. The peaks of E–G in the oligomer A are associated with the chemical structure of  $-\text{CH}_2\text{CF}_2\text{CH}_2\text{CF}_2\text{H}$  or  $\text{CH}_3\text{CF}_2-\text{CH}_2\text{CF}_2-$  as listed in Table 1.

Figure 2a shows  $^{13}\text{C}$  n.m.r. spectrum of the oligomer B. The chemical shifts of the peaks in the range 119–130 ppm show the hyperfine splitting with a splitting constant about 250–290 Hz. Some of these peaks split further with a splitting constant of 3.8 Hz as seen in Figure 2b. The chemical shifts of the peaks in the range 23–67 ppm show the hyperfine splitting with a splitting constant about 22 Hz. The other peaks are singlet.  $^{13}\text{C}$  spectra are divided into three groups of  $-\text{CH}_2-$ ,  $-\text{CF}_2-$  and the end groups. Based on the reference data<sup>10,11</sup>, the peaks in the range 23–67 ppm can be assigned to the resonances of  $-\text{CH}_2-$  groups. The hyperfine splitting about 22 Hz can be associated with the long range spin-spin interaction  $J_{\text{CCF}}^2$ . The splitting constants 250–290 Hz of the peaks in the range 119–130 ppm can be associated with the resonances of  $-\text{CF}_2-$  groups. The further splitting of the peaks about 3.8 Hz can be assigned to the long-range interaction  $J_{\text{CCCF}}^3$ .

The assignments of the peaks in the range of 23–67 ppm are easily determined based on the literature data<sup>10,11</sup>. The largest peak A' corresponds to the  $-\text{CH}_2-$  resonances in the normal head-to-tail structure. Peaks C and D correspond to the  $-\text{CH}_2-$  resonance in the head-to-head or tail-to-tail structure. The peaks of A' and C split into a pentuplet because of  $-\text{CF}_2-\text{C}^*\text{H}_2-\text{CF}_2-$  structure. Peak D splits into triplet because of the  $-\text{CH}_2-\text{C}^*\text{H}_2-\text{CF}_2-$  structure. The peaks K' and H' are assigned to the  $-\text{CH}_2-$  groups linked with  $\text{CCl}_3-$  and  $\text{Cl}-$ , respectively, at the chain ends. According to their hyperfine splittings, the peak K' with triplet splitting is

assigned to the  $\text{CCl}_3-\text{C}^*\text{H}_2\text{CF}_2-$  structure. Peak H' with pentuplet splitting is assigned to the  $-\text{CF}_2-\text{CH}_2-\text{CF}_2-\text{Cl}$  structure. The assignments of the peaks in the range 119–130 ppm can be determined also based on the reference data<sup>10,11</sup>. The largest peak A in Figure 2b corresponds to the signal of  $-\text{CF}_2-$  arranged in the head-to-tail structure. However, the peaks corresponding to the head-to-head or tail-to-tail structure cannot be detected because of very weak peak intensities and overlapping with the hyperfine structure of the other peaks. The peaks H–K can be related to the  $-\text{CF}_2-$  groups located near to the chain ends. Based on the splitting constant (about 290 Hz), peak H–J can be assigned to the  $-\text{CF}_2-$  groups attached to the Cl atom. Further splits in the peak H into triplet but not in the peak I (singlet) indicate the tail-to-tail structure such as  $-\text{CH}_2\text{CF}_2-\text{CF}_2\text{CH}_2-\text{CH}_2\text{C}^*\text{F}_2-\text{Cl}$  for I and the head-to-tail structure such as  $-\text{CH}_2\text{CF}_2-\text{CH}_2\text{CF}_2-\text{CH}_2\text{C}^*\text{F}_2-\text{Cl}$  for H. Based on the splitting constant of about 246 Hz in peaks J and K and further splitting in the peak K into triplet but not in peak J (singlet), peaks of J and K can be assigned to the structure  $-\text{CH}_2\text{CF}_2-\text{CH}_2\text{C}^*\text{F}_2-\text{CH}_2\text{CF}_2-\text{Cl}$  and  $\text{CCl}_3-\text{CH}_2\text{C}^*\text{F}_2-\text{CH}_2\text{CF}_2-\text{CH}_2\text{CF}_2-$ , respectively. Peak L is associated with the chain end of  $\text{CCl}_3-$ . The other peaks with singlet can be related to the resonances from the chemical structure of the fragment of the initiator. The detailed assignments of these peaks are listed in Table 1 together with the results from  $^{19}\text{F}$  n.m.r. spectra. The formation of the double bond groups at the chain ends can be neglected for the telomerization of VDF monomer for the oligomers B and C and for the decomposition in the vacuum deposition process for the oligomer A, since no signal for the double bond groups is observed in n.m.r. spectra.

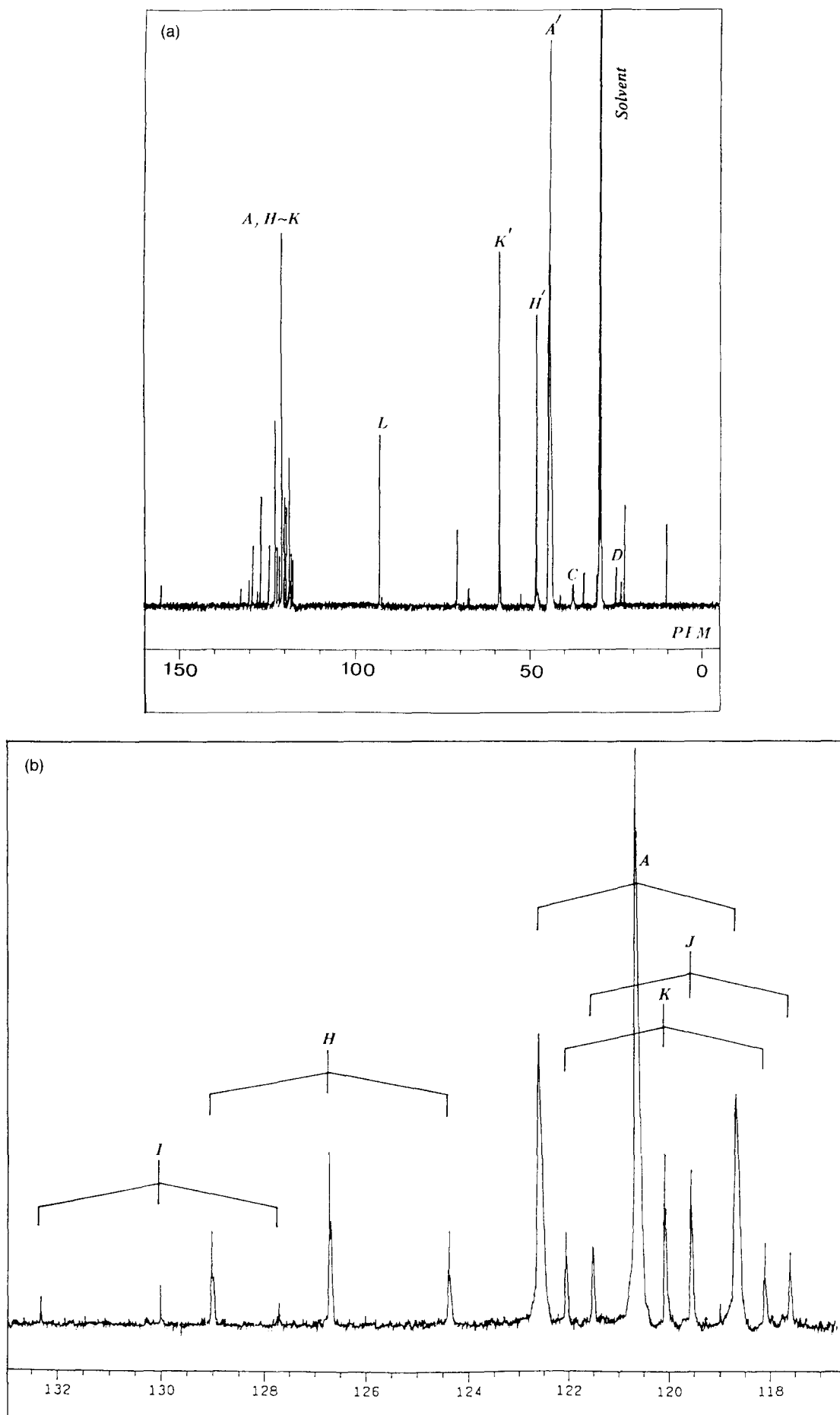
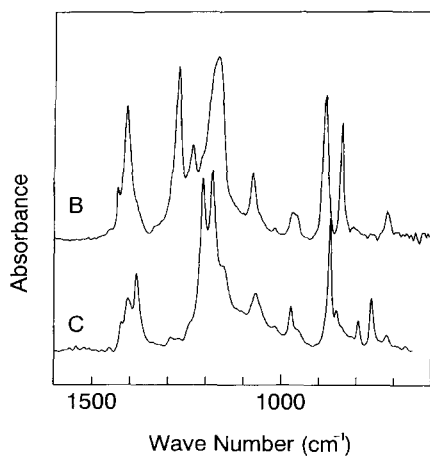
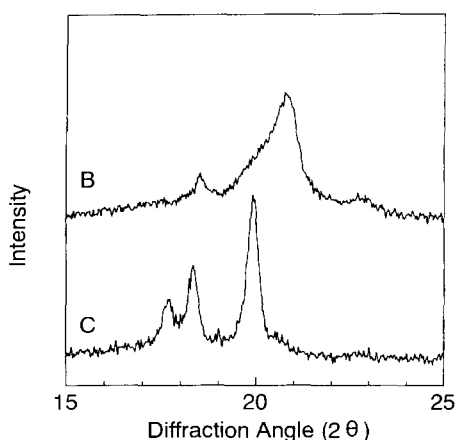


Figure 2 <sup>13</sup>C n.m.r. spectra of oligomer B (a) and the further splits in the peaks of A and H K



**Figure 3** The i.r. spectra of two oligomers B and C casting from acetone solution on to silicon wafer substrate



**Figure 4** X-ray diffraction patterns of two oligomers B and C casting from acetone solution on to silicon wafer substrate

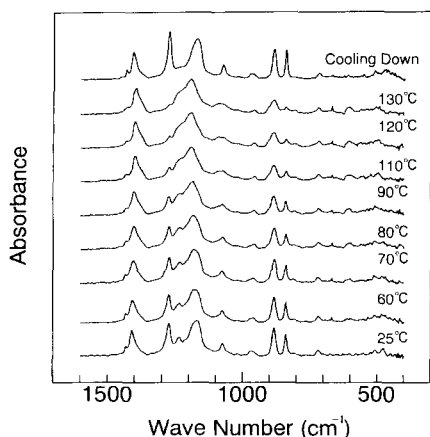


**Figure 5** *In situ* i.r. measurements of oligomers B in KBr disk at various temperatures

The degree of the structural imperfections (h-h and t-t) and the degree of polymerization are estimated from the above n.m.r. results listed in Table 2. The degrees of structural defects are in the range 4–7%, which is in good agreement with the reported data<sup>1,7,9</sup>. The degree of polymerization for oligomers A, B and C are about 20, 9 and 20, respectively, which agree with those values obtained by elemental analysis. When these oligomers

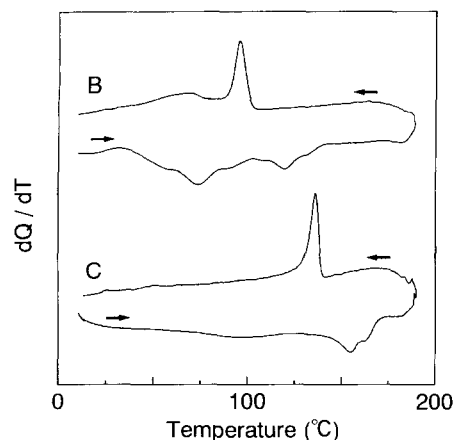


**Figure 6** D.s.c. curves of two oligomers B and C. The arrows indicate the directions of heating and cooling processes

were vapour-deposited onto the silicon wafer substrate kept at room temperature, the films exhibited a layer-by-layer structure with the normal molecular orientation to the substrate. There was a sharp diffraction peak associated with the (001) reflection for each oligomer. The spacings calculated from the diffraction peaks were 4.9 nm for the oligomer A, 2.7 nm for the oligomer B and 5.0 nm for the oligomer C. These spacings are consistent with the degree of polymerization obtained by n.m.r. listed in Table 2.

Figure 3 and Figure 4 show i.r. spectra and X-ray diffraction patterns for the oligomers of B and C cast from acetone solution. The oligomer C shows a typical  $\alpha$  form in i.r. spectra exhibiting the characteristic absorption bands as  $1212\text{ cm}^{-1}$  and  $1185\text{ cm}^{-1}$ . The X-ray diffraction pattern shows three sharp peaks at  $2\theta = 17.7^\circ$ ,  $18.3^\circ$  and  $19.9^\circ$ , respectively, corresponding to (100), (020) and (110) for the  $\alpha$  form. The cast-film of the oligomer A from acetone solution also showed the  $\alpha$  form. In general, the  $\alpha$  form can be obtained when PVDF is cast from acetone solution<sup>1</sup>. The cast-film of the oligomer B shows a mixture of the  $\beta$  and the  $\gamma$  forms exhibiting the characteristic bands at  $1278\text{ cm}^{-1}$  for the  $\beta$  form and at  $1236\text{ cm}^{-1}$  for the  $\gamma$  in Figure 3 and the peaks at  $2\theta = 21^\circ$  for the  $\beta$  crystal and  $2\theta = 18^\circ$  for the  $\gamma$  crystal in Figure 4. However, the amount of the  $\beta$  form is larger than that of the  $\gamma$  form.

Figure 5 shows the temperature dependence of i.r. spectra (*in situ* measurement) for the oligomer B prepared on a KBr disk. The original sample is consistent of the mixture of the  $\beta$  and the  $\gamma$  forms. The peak intensity at  $1278\text{ cm}^{-1}$  associated with the  $\beta$  form decreases with an increase in temperature and disappears at about  $100^\circ\text{C}$  although not completely. Optical microscopy studies indicated the melting of the small crystals starting from about  $90^\circ\text{C}$  to  $100^\circ\text{C}$  with diminishing the number of their crystals. Above  $100^\circ\text{C}$ , the crystal size reduced with an increase in temperature and the crystals disappeared completely above  $130^\circ\text{C}$ . These results are supported by d.s.c. data as shown in Figure 6. Two melting peaks at about  $80^\circ\text{C}$  and  $117^\circ\text{C}$  and two crystallization peaks at  $102^\circ\text{C}$  and  $67^\circ\text{C}$  are found for the oligomer B. According to the results of g.p.c.<sup>4</sup>, the oligomer B showed a double molecular weight distribution. These two molecular weight components are crystallized individually at  $102^\circ\text{C}$  and  $67^\circ\text{C}$ . It is interesting to note that the almost perfect  $\beta$  form is

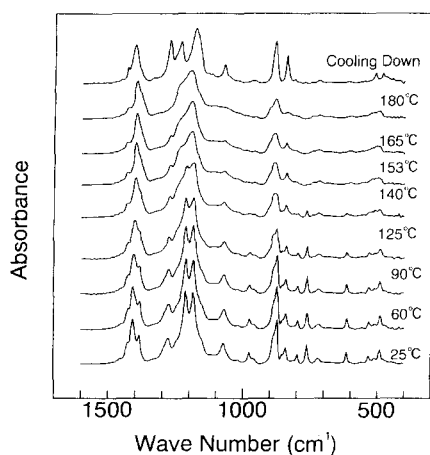


**Figure 7** *In situ* i.r. measurements of oligomer C in KBr disk at various temperatures

**Table 2** The most probable chemical structures, the percentage of head-to-tail monomer sequences (h-t) and the degree of polymerization (*n*) for the VDF oligomers

Sample	Chemical structure	H-T (%)	<i>n</i>
PVDF	$-(\text{CH}_2\text{CF}_2)_n-$	94.5	300 (g.p.c.)
VDF-A	$\text{In}-(\text{CH}_2\text{CF}_2)_n-\text{H}$	92.9	20 (n.m.r.)
VDF-B	$\text{CCl}_3-(\text{CH}_2\text{CF}_2)_n-\text{Cl}$	96.0	9 (n.m.r. & AN)
VDF-C	$\text{CCl}_3-(\text{CH}_2\text{CF}_2)_n-\text{Cl}$	93.5	20 (n.m.r. & AN)

G.p.c.: estimated from g.p.c.

N.m.r.: estimated from n.m.r. in this work

AN: estimated from an elemental analysis

**Table 3** Crystal forms and melting temperatures for VDF oligomers

Sample	From acetone <sup>a</sup>	From bulk <sup>b</sup>	<i>T<sub>m</sub></i> (°C)
PVDF	α	α	182
VDF-A	α	α	130
VDF-B	β with γ	β with γ	74/110
VDF-C	α	γ	155

<sup>a</sup> Casting from acetone solution on to silicon wafer

<sup>b</sup> Crystallized from molten state by cooling down to room temperature

observed when the sample is cooled to room temperature from the molten state in a KBr disk. This indicates that the oligomer B is crystallized in the β form in the KBr disk, since this form is obtained by epitaxial melt crystallization on KBr<sup>1</sup>.

Figure 7 shows the temperature dependence of i.r. (*in situ* measurement) for the oligomer C. It is found that the i.r. band at 1278 cm<sup>-1</sup> for the β form whereas the original oligomer C shows only the bands corresponding to the α form. This result suggests that the β form in the KBr disk can be formed during the sample preparation such as grinding the sample with KBr powder. The peaks at 1212 cm<sup>-1</sup> and 1815 cm<sup>-1</sup> corresponding to the α form decrease with an increase in temperature and disappear at about 140°C. There is a single melting peak at about 155°C with a small shoulder peak at about 160°C (see Figure 6). The optical microscopy studies indicated that the birefringence of the crystals began to disappear up to 150°C and the crystals were completely melted above 160°C. These results suggest that the d.s.c. peak at 155°C

is attributed to the melting of the α form and the shoulder peak at 160°C can be associated with the melting of the hexagonal form. That is, the α form is transferred to the hexagonal form such as a rotator phase which is often observed in a linear long chain molecule, such as a paraffin<sup>12</sup>. In fact, the rotator phase is reported in VDF oligomer with the degree of polymerization of about nine and with the iodine chain-end detected by an energy dispersive-type total reflection X-ray diffractometer<sup>13</sup>. The VDF oligomer terminated with iodine shows the γ form when the oligomer is crystallized from the melt and the α form when the oligomer is vapour-deposited on the substrate. The crystalline phase transition from the α form to the γ form occurs at about 70°C. When the oligomer C is cooled down to room temperature from the molten state in KBr disk, the mixture of the β and the γ forms are observed as seen in Figure 7. The mixture crystals are caused from the epitaxial crystallization in KBr disk for the β form and the chain end effect for the γ form.

These results discussed above can be associated with the effects of the chain ends and the low degree of polymerization. That is, the large or massive chain end groups will induce the chain distortion in the molecules yielding the γ form when the oligomers are crystallized from the melt, since the oligomers A and C have almost the same degree of polymerization, as listed in Table 2. The shorter the chain length of the VDF oligomer gives rise to the β form by comparing oligomer B with oligomer C, as listed in Table 2 and Table 3. On the other hand, the large end-group results in the γ form because the oligomer with the iodine end group shows the γ form and oligomer B shows a mixture of the β and the γ forms; these two oligomers have almost the same chain length. It is interesting to note that the massive chain end groups give rise to the high melting temperature by comparing the oligomer A with the oligomer C which are almost the same chain length. This means that the entropy of melting decreases with an increase in the weight of the chain end group, because of suppression of the chain mobility by the heavy chain end group in the melt.

## ACKNOWLEDGEMENTS

The authors are grateful to Mr N. Bannai of Kureha Chemical Industry Co. Ltd for preparing the oligomers of B and C and to Mr Y. Nakamura of Tokyo Institute of Technology for measuring n.m.r. spectra.

## REFERENCES

- 1 Lovinger, A. J. in 'Developments in Crystalline Polymers—1', (Ed. Bassett D. C.), Applied Science Publishers, London, 1982, p. 195
- 2 Hsu, C. C. and Geil, P. H., *J. Appl. Phys.* 1984, **56**, 2404
- 3 Takeno, A., Okui, N., Kitoh, T., Muraoka, M., Umemoto, S. and Sakai, T. *Thin Solid Films* 1991, **202**, 205
- 4 Takeno, A., Okui, N., Hiruma, T., Kitoh, T., Muraoka, M., Umemoto, S. and Sakai, T. *Kobunshi Ronbunshu* 1991, **48**, 399
- 5 Takeno, A., Okui, N., Hiruma, T., Muraoka, M., Umemoto, S. and Sakai, T. *Kobunshi Ronbunshu* 1991, **48**, 405
- 6 Wilson III, C. W. and Santee Jr. E. R. *J. Polym. Sci., Part C* 1965, **8**, 97
- 7 Ferguson, R. C. and Brame Jr., E. G. *J. Phys. Chem.* 1979, **83**, 1397

- |    |   |    |  |
|----|---|----|--|
| 8  | Tonelli, A. E., Schilling, F. C. and Cais, R. E., <i>Macromolecules</i> <b>15</b> , 849                         | 11 | Tonelli, A. E., Schilling, F. C. and Cais, R. E., <i>Macromolecules</i> 1981, <b>14</b> , 560                                  |
| 9  | Russo, S., Behari, K., Cheng, S., Pianca, M., Barchiesi, E. and Moggi, G. <i>Polymer</i> 1993, <b>34</b> , 4777 | 12 | Ewen, B., Strobl, G. R. and Richter, D. <i>Faraday Discuss. Chem. Soc.</i> 1980, <b>69</b> , 19                                |
| 10 | Bovey, F. A., Schilling, F. C., Kwei, T. K. and Frisch, H. L., <i>Macromolecules</i> 1977, <b>10</b> , 559      | 13 | Yoshida, Y., Ishizaki, K., Horiuchi, T. and Matshige, K. <i>Reports on Progress in Polym. Phys. Jpn.</i> 1993, <b>36</b> , 225 |